Report

Current Biology

SHOU4 Proteins Regulate Trafficking of Cellulose Synthase Complexes to the Plasma Membrane

Graphical Abstract

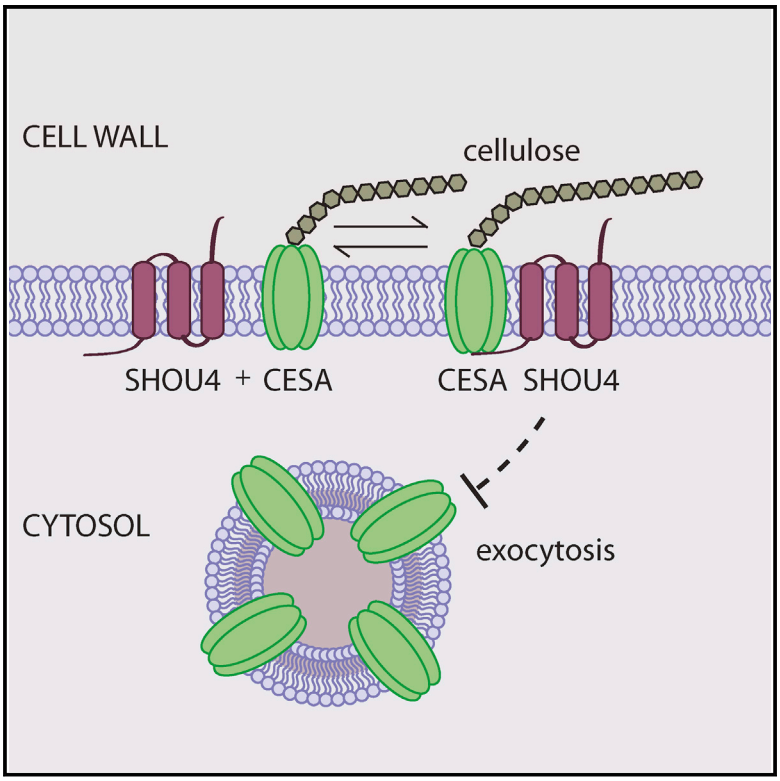

Authors

Joanna K. Polko, William J. Barnes, Cătălin Voiniciuc, ..., Markus Pauly, Charles T. Anderson, Joseph J. Kieber

Correspondence

jkieber@unc.edu

In Brief

The regulation of the intracellular trafficking of cellulose synthase (CESAs) complexes plays a crucial role in modulating the level of cellulose synthesis in plants. Polko et al. identify two paralogous novel plasma-membrane-localized proteins that negatively regulate cellulose synthesis by inhibiting the exocytosis of CESAs.

Highlights

- Disruption of *SHOU4/4L* genes suppresses mutants with decreased cellulose
- *shou4 shou4l* mutants have increased levels of amorphous cellulose
- SHOU4/4L are novel plant proteins that interact with cellulose synthases (CESAs)
- SHOU4 proteins negatively regulate CESA exocytosis

Polko et al., 2018, Current Biology *28*, 1–9
October 8, 2018 © 2018 Elsevier Ltd.
https://doi.org/10.1016/j.cub.2018.07.076

CellPress

Please cite this article in press as: Polko et al., SHOU4 Proteins Regulate Trafficking of Cellulose Synthase Complexes to the Plasma Membrane, Current Biology (2018), https://doi.org/10.1016/j.cub.2018.07.076

Current Biology
Report

CellPress

SHOU4 Proteins Regulate Trafficking of Cellulose Synthase Complexes to the Plasma Membrane

Joanna K. Polko,[1] William J. Barnes,[2] Cătălin Voiniciuc,[3] Stephanie Doctor,[1] Blaire Steinwand,[1] Joseph L. Hill, Jr.,[4,5] Ming Tien,[4] Markus Pauly,[3] Charles T. Anderson,[2] and Joseph J. Kieber[1,6,*]
[1]Department of Biology, University of North Carolina, Chapel Hill, Chapel Hill, NC 27599, USA
[2]Department of Biology, Pennsylvania State University, University Park, PA 16802, USA
[3]Institute of Plant Cell Biology and Biotechnology, Heinrich-Heine University Düsseldorf, Düsseldorf, Germany
[4]Department of Biochemistry and Molecular Biology, Pennsylvania State University, University Park, PA 16802, USA
[5]Present address: Department of Horticulture, Michigan State University, East Lansing, MI 48824, USA
[6]Lead Contact
*Correspondence: jkieber@unc.edu
https://doi.org/10.1016/j.cub.2018.07.076

SUMMARY

Cell walls play critical roles in plants, regulating tissue mechanics, defining the extent and orientation of cell expansion, and providing a physical barrier against pathogen attack [1]. Cellulose microfibrils, which are synthesized by plasma membrane-localized cellulose synthase (CESA) complexes, are the primary load-bearing elements of plant cell walls [2]. Cell walls are dynamic structures that are regulated in part by cell wall integrity (CWI)-monitoring systems that feed back to modulate wall properties and the synthesis of new wall components [3]. Several receptor-like kinases have been implicated as sensors of CWI [3–5], including the FEI1/FEI2 receptor-like kinases [4]. Here, we characterize two genes encoding novel plant-specific plasma membrane proteins (SHOU4 and SHOU4L) that were identified in a suppressor screen of the cellulose-deficient *fei1 fei2* mutant. *shou4 shou4l* double mutants display phenotypes consistent with elevated levels of cellulose, and elevated levels of non-crystalline cellulose are present in this mutant. Disruption of *SHOU4* and *SHOU4L* increases the abundance of CESA proteins at the plasma membrane as a result of enhanced exocytosis. The SHOU4/4L N-terminal cytosolic domains directly interact with CESAs. Our results suggest that the SHOU4 proteins regulate cellulose synthesis in plants by influencing the trafficking of CESA complexes to the cell surface.

RESULTS

Disruption of the *FEI1* and *FEI2* receptor-like kinases (RLKs) results in a range of cell-wall-related phenotypes as a result of decreased cellulose levels, including short and swollen roots in the presence of elevated sucrose or salt, hypersensitivity to the cellulose biosynthesis inhibitor isoxaben, thickened hypocotyls and stamens, and impaired formation of cellulose rays in seed mucilage [4, 5]. In order to identify new elements regulating cell wall synthesis, we screened for genetic suppressors of the *fei1 fei2* swollen root phenotype and identified the *shou4-1* mutant (Figures 1A, 1B, and S1A). *shou4-1* also suppressed *fei1 fei2* when heterozygous, indicating that it is dominant (Figure 1B). Next-generation mapping revealed that *shou4-1* resulted from a transition mutation in an intron donor site in the gene At1g78880 that leads to the adoption of a cryptic splice site. The resultant mRNA encodes a predicted protein with a 15-amino-acid deletion relative to the wild-type (Figures 1C and S1B). Introduction of a wild-type *SHOU4* genomic transgene (fused to a GFP or mCherry reporter) into a *fei1 fei2 shou4-1* line resulted in a full or partial reversion of the *shou4* suppression (Figures S1F and S1G). Characterization of a T-DNA insertional allele, *shou4-3*, also confirmed that At1g78880 corresponds to *shou4* (Figures 1C, S1A, and S1C). Similar to *shou4-1*, the *shou4-3* allele is also dominant (Figure S1E). The dominant nature of the *shou4* mutations coupled with the hypomorphic nature of the *shou4-3* allele (Figures 1B, S1D, and S1E) indicates that *SHOU4* is haploinsufficient. We examined whether *shou4-1* reverts other cellulose-deficient mutants and found that it suppressed or partially suppressed the root swelling phenotypes of *procuste1* (*cesa6*^{prc}) [6] and *salt overly sensitive5* (*sos5*) [7], but not *cobra* [8] (Figures 1D, 1E, and S1H).

SHOU4 and Its Paralog, SHOU4L, Are Novel Plant-Specific Proteins that Modulate Cell Wall Function

SHOU4 encodes a novel protein with no regions of homology to any domains of known function. SHOU4 is predicted to have three transmembrane domains with a cytosolic N terminus (Figures 2A and S2A). Consistent with this topology prediction, we observed that SHOU4 is localized primarily to the plasma membrane (PM) and does not bind strongly to the cell wall as the majority is retained in the PM following plasmolysis (Figures S2E and S2F). The remnant cell-wall-localized GFP signal likely corresponds to Hechtian strands [11]. SHOU4 is broadly expressed, with the highest level of expression in root tips, the vasculature, and the center of the rosette (Figure S2G). In *Arabidopsis*, SHOU4 has a close paralog (89% amino acid identity) that we have named SHOU4-like (SHOU4L; At1g16860), as well as a more distant paralog (SHOU4L2; At4g22290; 49% amino acid identity; Figures 2A, 2B, and S2A). Orthologs of SHOU4 are

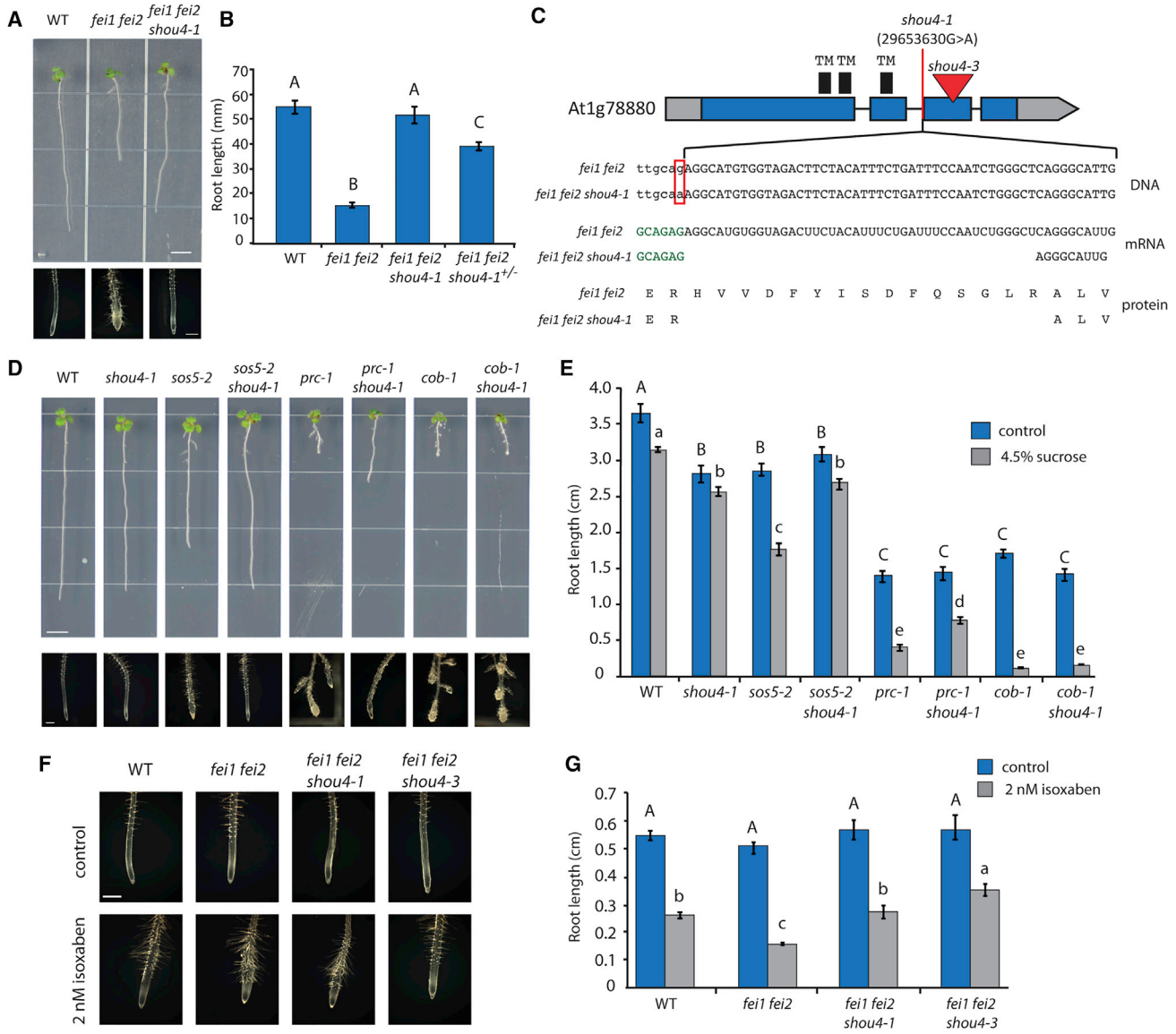

Figure 1. Mutations in *shou4* Suppress Cell Wall Defects

(A) *shou4-1* suppresses the *fei1 fei2* mutant phenotype. Seedlings were grown for 14 days on media containing 4.5% sucrose. The bottom panels show a close up of the root tips.

(B) Quantification of root length from seedlings grown as in (A). *fei1 fei2 shou4-1*$^{+/-}$ indicates an F1 progeny of a cross between *fei1 fei2 shou4-1* and *fei1 fei2*.

(C) Gene model of *SHOU4* (At1g78880) with the boxes representing exons and the blue indicating the coding region. The *shou4-1* mutation (G →A, red box) is in the 2nd intron leading to an in-frame deletion of 45 nt (exon 3). Nucleotides depicted in green represent sequences derived from exon 2. The position of the T-DNA insertion in the *shou4-3* allele is also indicated.

(D) Suppression of cell wall defects in other cellulose deficient mutants by *shou4-1*. Four-day-old seedlings were transferred from control media to 4.5% sucrose media and the subsequent root growth measured after five days. The bottom panels show a close-up of the root tips.

(E) Quantification of root length from seedlings shown in (D).

(F and G) Mutations in *SHOU4* suppress hypersensitivity of *fei1 fei2* to isoxaben that is manifested by radial root swelling (F) and root shortening (G). For (G), four-day-old seedlings were transferred to media containing 2 nM isoxaben and the increase in root length was measured after 24 hr. Values are means ($n > 10$) ± SEM. Different letters indicate significant differences with lowercase and uppercase letters representing separate analyses.

Data were analyzed with one-way ANOVA and Tukey-Kramer post hoc comparisons; $p < 0.05$. The scale bars represent 5 mm for upper panel (A and D) and 0.5 mm for lower panel (A, D, and F). See also Figure S1.

present in rice (*Oryza sativa*), the basal angiosperm *Amborella trichopoda*, the lycophyte *Selaginella moelledorffii*, and the moss *Physcomitrella patens* (Figure 2B) but are not found in green algae or in animal or fungal genomes.

Disruption of *SHOU4L* also suppressed the root swelling phenotype of *fei1 fei2* (Figures S2B–S2D). A double *shou4-3 shou4l-1* mutant has a wide range of phenotypic defects that are either absent or much milder in the single mutants,

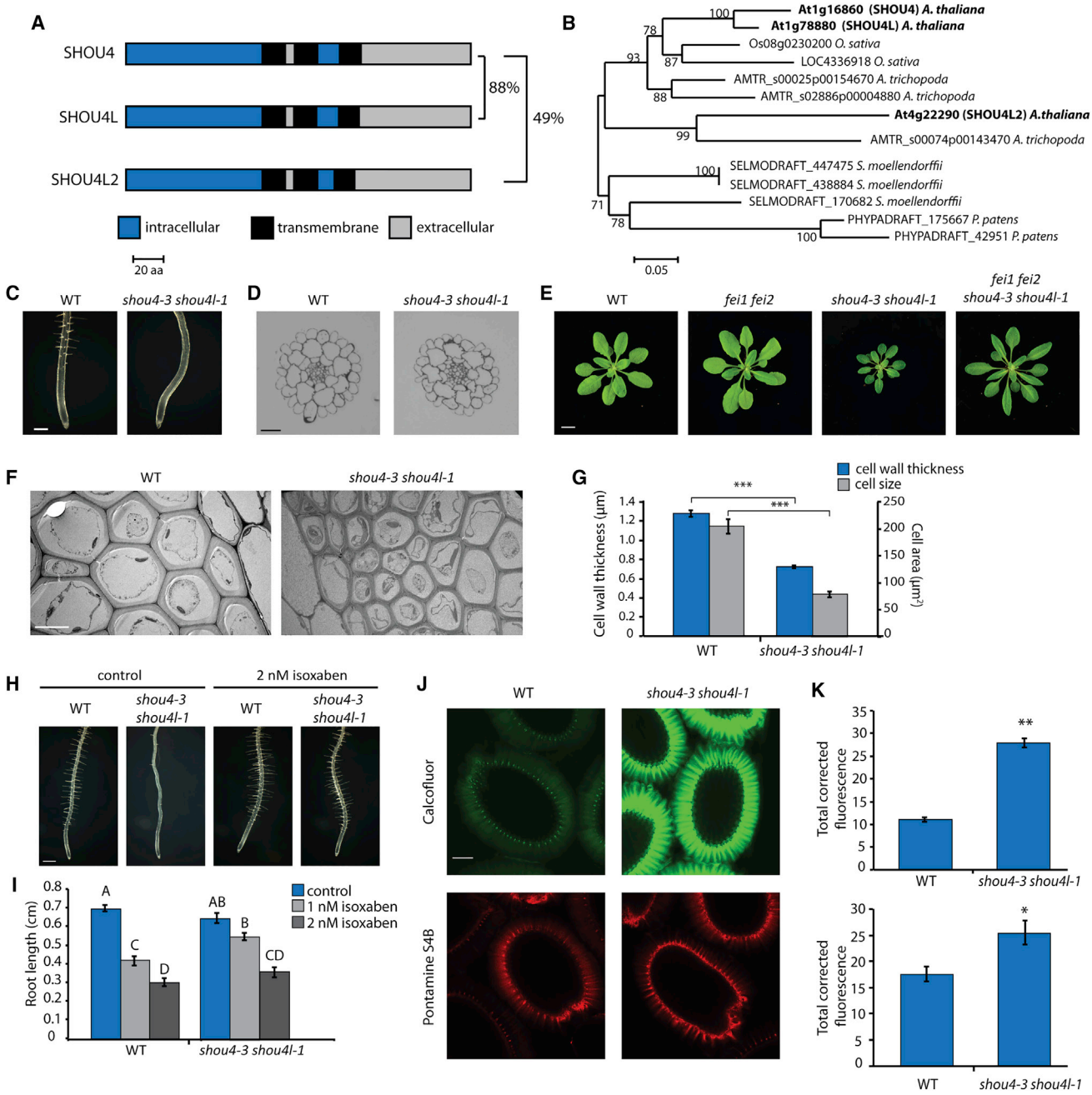

Figure 2. *SHOU4* Encodes a Novel Transmembrane Protein Involved in Cell Expansion and Cell Wall Synthesis

(A) Protein models of SHOU4 (At1g78880), SHOU4L (At1g16860), and SHOU4L2 (At4g22290). The % amino acid identity between the proteins is indicated on the right. The alignment was generated with PSI/TM-Coffee package [9] (note that other transmembrane [TM] domain tools, such as Protter [10], predict two TM domains).

(B) Neighbor-joining tree of SHOU4 homologs from *Arabidopsis*, *Oryza sativa*, *Amborella trichopoda*, *Physcomitrella patens*, and *Selaginella moellendorffii.*

(C) Root tips of wild-type (WT) and *shou4-3 shou4l-1* mutants. Note the lack of root hairs in the mutant.

(D) Cross section of the root elongation zone of seven-day-old seedlings.

(E) 30-day-old rosettes of plants of the indicated genotypes.

(F) Transmission electron microscopy (TEM) images of interfascicular fibers in inflorescence stems from 37-day-old plants grown in long days.

(G) Measurements of the secondary cell wall thickness and cell size of interfascicular fiber cells from (F). Values are means ($n > 29$) ± SEM. Data were analyzed by unpaired Student's t test. Asterisks indicate significant differences relative to the WT; ***$p < 0.001$.

(H) Short-term isoxaben treatment induces root hair development in *shou4-3 shou4l-1* roots. Four-day-old seedlings were transferred to media containing 2 nM isoxaben for 18 hr.

(I) Quantification of root length in response to 18 hr isoxaben treatment. Data were analyzed with one-way ANOVA and Tukey-Kramer post hoc comparisons; $p < 0.05$; $n > 9$.

(legend continued on next page)

suggesting partial functional redundancy. Additional loss of function in *SHOU4L2* does not further enhance these phenotypes (Figure S3A). At the seedling stage, the *shou4-3 shou4l-1* double mutants have very few root hairs, and those that are present are underdeveloped. *shou4-3 shou4l-1* roots grow with a slight twist, but there are no major differences in cellular organization in the elongation zone (Figures 2C and 2D). Moreover, *shou4-3 shou4l-1* double mutants are dwarf with smaller rosettes (Figures 2E and S3A) and inflorescences. We examined cells in cross sections of wild-type and *shou4-3 shou4l-1* double-mutant inflorescence stems. In general, in the double mutant, cells are smaller and have thinner cell walls (Figures 2F and 2G). Furthermore, in *shou4-3 shou4l-1* double mutants, the papillae on the surface of the stigma are substantially underdeveloped, which likely contributes to the partial infertility of the double mutant (Figures S3B and S3C). The *fei1 fei2 shou4-3 shou4l-1* quadruple mutant was comparable in size to the wild-type (Figure 2E), which indicates that disruption of *FEI1* and *FEI2* suppresses the dwarfism of *shou4-3 shou4l-1.* This indicates that FEI1 and FEI2 act throughout development to modulate cell wall synthesis.

Isoxaben inhibits cellulose biosynthesis and induces radial cell swelling in rapidly growing cells [12]. *fei1 fei2* mutant roots, which have reduced cellulose biosynthesis, are hypersensitive to isoxaben [4], and this is suppressed by *shou4* mutations (Figures 1F, 1G, and S1I). In contrast to *fei1 fei2*, the *shou4-3 shou4l-1* double mutant displays reduced sensitivity to isoxaben as compared to the wild-type in both roots and etiolated hypocotyls (Figures 2H, 2I, S2H, S3D, and S3E). Short-term exposure of *Arabidopsis* hypocotyls to isoxaben increases the occurrence of small CESA compartments (SmaCCs) or microtubule-associated cellulose synthase compartments (MASCs) [13–15]. We tested whether the uniform PM distribution of SHOU4 was altered upon isoxaben treatment but observed no substantial changes in SHOU4 localization (Figure S3F). Remarkably, treatment with a low concentration of isoxaben reverted the root hair defects of *shou4-3 shou4l-1* seedlings (Figure 2H). Root hair development is initiated by a local wall acidification and expansin-dependent, site-specific cell wall loosening in trichoblasts [16, 17].

Arabidopsis seeds contain a mucilage layer on their surface that is released upon seed imbibition. This mucilage is composed primarily of pectin but also contains hemicelluloses and cellulose that play important structural roles [5, 18]. Cellulosic rays anchor a portion of the mucilage to the seed surface and can be visualized by staining with either calcofluor or Pontamine Fast S4B [19]. Cellulose-deficient mutants, such as *cesa5*, *sos5*, *fei2*, or *cobl2*, have reduced levels of calcofluor and Pontamine S4B staining in seed coat mucilage [5, 20] that reflects reduced cellulose ray formation. In contrast to these mutants, *shou4-3 shou4l-1* seeds showed significantly increased calcofluor and Pontamine S4B fluorescence (Figures 2J and 2K), suggesting that their mucilage contains elevated levels of cellulose.

In sum, these results suggest that SHOU4 proteins negatively regulate cellulose synthesis based on: (1) *shou4* and *shou4l* mutations suppress the phenotypes of mutants with reduced cellulose; (2) the dwarf *shou4 shou4l* phenotype is reverted by *fei1 fei2*, mutations that reduce cellulose biosynthesis; (3) the *shou4 shou4l* mutant is less sensitive to the cellulose inhibitor isoxaben; (4) disruption of *SHOU4*/*SHOU4L* inhibits root hair emergence, and this is reversed by treatment with isoxaben; and (5) the double *shou4 shou4l* mutant displays increased cellulose levels in seed mucilage. Thus, we analyzed cellulose levels in the *shou4 shou4l* mutant.

shou4 shou4l Mutants Have Elevated Levels of Amorphous Cellulose

Contrary to our expectations, the amounts of crystalline cellulose in the double *shou4-3 shou4l-1* mutant was comparable to that of wild-type (Figure 3A). Nevertheless, the cell walls of double-mutant shoots contained significantly more glucose than wild-type but comparable quantities of all other monosaccharides (Figure 3B). The only polysaccharides in these cell wall extracts that are comprised solely of glucose are callose and amorphous cellulose. Callose levels in the mutant are comparable to those in the wild-type (Figure S3G). Amorphous cellulose can be detected using *Bacillus*-derived carbohydrate binding module 28 (CBM28) [22, 23]. We conducted immunocytochemistry using His-tagged recombinant CBM28 coupled with immunogold-labeled anti-His antibodies [24]. Within the secondary cell walls of the interfascicular fibers, CBM28 binding was more abundant in the *shou4-3 shou4l-1* mutant (Figures 3C and 3D), which, together with our other data, suggests that disruption of *SHOU4* and *SHOU4L* results in elevated levels of amorphous cellulose.

SHOU4 Proteins Control Abundance at the PM through Negatively Regulating CESA6 Exocytosis

In vascular plants, cellulose is organized into microfibrils that are synthesized by PM-localized cellulose synthase (CESA) complexes (CSCs) that move along cortical microtubules [25]. Primary cell wall microfibrils are synthesized by CSCs that contain CESA1, CESA3, and CESA6-like proteins, whereas the cellulose in secondary cell walls is made by CESA4, CESA7, and CESA8 [2].

Neither *CESA* transcript nor protein levels were elevated in the *shou4-3 shou4l-1* mutant (Figures S4A–S4D). However, measurements of the CESA6-yellow fluorescent protein (YFP) particles in epidermal cells in the root elongation zone revealed that there was increased particle abundance at the PM in the double *shou4-3 shou4l-1* mutant that was exacerbated when seedlings were transferred to media containing elevated sucrose (Figures 4A and 4B). Wild-type root cells responded to elevated sucrose concentrations by internalizing CESA6-YFP, whereas CESA6-YFP in the *shou4-3 shou4l-1* background was insensitive to exogenous sucrose. We also observed a similar increase in

(J) Confocal micrographs of imbibed WT and mutant seeds stained with calcofluor (top) and Pontamine Fast Scarlet S4B (bottom).
(K) Quantification of results shown in (J). Values are means ($n > 8$) ± SEM.
Data were analyzed by unpaired Student's t test. Asterisks indicate significant differences relative to the WT; *$p < 0.05$; **$p < 0.01$. The scale bars represent 250 μm for (C), 100 μm for (D), 1 cm for (E), 10 μm for (F), 500 μm for (H), and 1 mm for (J). See also Figures S2 and S3.

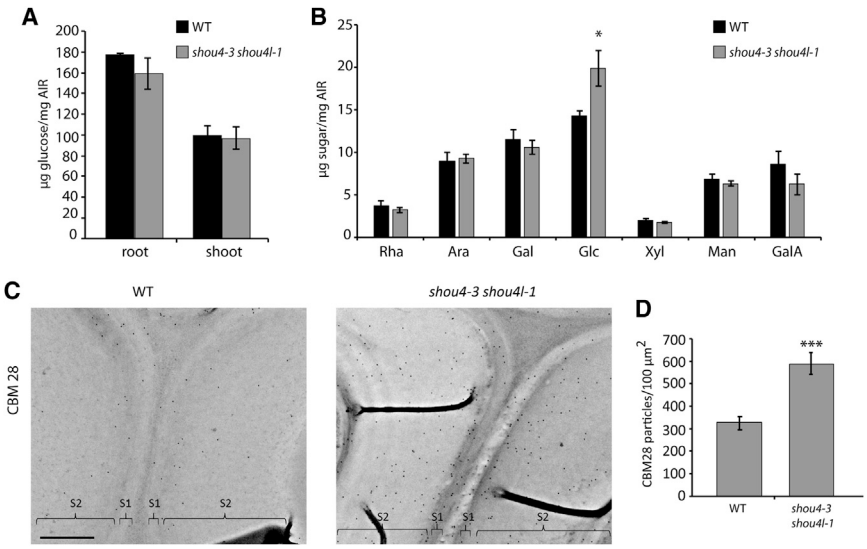

Figure 3. *shou4 shou4l* Mutants Display Increased Levels of Amorphous Cellulose

(A) Crystalline cellulose content in 10-day-old roots and shoots measured by the Updegraff method [21]. AIR, alcohol-insoluble residue.

(B) Monosaccharide composition of de-starched ten-day-old shoots. Both datasets indicate means ± SEM (n = 3 biological replicates) and were analyzed by unpaired Student's t test. Asterisks indicate significant differences relative to the WT; *p < 0.05.

(C) Representative TEM micrographs showing secondary cell walls of the interfascicular fibers of inflorescence stems after immunogold labeling using CBM28. White arrowheads indicate the gold particles. S1 and S2 indicate different sublayers of the secondary cell wall. The scale bar represents 2 µm.

(D) Quantification of data shown in (C). Density of gold particles was measured from n > 40 cells from 2 plants ± SEM.

Data were analyzed by unpaired Student's t test. Asterisks indicate significant differences relative to the WT; ***p < 0.001. See also Figure S3.

CESA6-YFP signal in epidermal cells of etiolated hypocotyls (Figure 4C) grown in the absence of sucrose, which we subsequently used as a model for studying CESA6-YFP trafficking. The increased CESA abundance, however, did not result in changes in the velocity of CESA particles in the mutant (Figures S4E and S4F; Video S1). Despite comparable velocities, we noticed that CESA6-YFP particles in *shou4-3 shou4l-1* mutants traveled along more closely aligned paths. Subsequent measurements of particle directionality showed that, despite unchanged average trajectory angles (wild-type [WT] 45.1° ± 2.3°; *shou4-3 shou4l-1* 44.4° ± 1.8°), the variance of the trajectory angles was smaller in *shou4-3 shou4l-1* (Figures S4G and S4H). These results suggest that the higher density of the CESA particles in the *shou4-3 shou4l-1* mutant increases the probability that the movement of one particle influences the trajectory of adjacent particles.

These results suggest that SHOU4 and SHOU4L likely influence trafficking of CESA proteins between the PM and intracellular compartments. We used fluorescent recovery after photobleaching (FRAP) to quantify the rate of exocytosis of CESA proteins to the PM [15, 27]. In WT hypocotyls, we observed a delivery rate of approximately 6 particles/$\mu m^2 hr^{-1}$, consistent with previous observations [15] (Figure 4D; Video S2). The *shou4-3 shou4l-1* double mutant displayed a significant increase in the rate of particle delivery (Figure 4D), suggesting that the increased density of CESA6-YFP at the PM in the mutant is the result of an increased rate of exocytosis. We assessed a delivery rate of a different PM protein, PIN1, and observed a slight, non-significant, decrease in FRAP of PIN1-GFP in the double *shou4-3 shou4l-1* mutant (Figure S4I). Based on these results, we conclude that the WT SHOU4 and SHOU4L proteins negatively regulate CESA delivery to the PM.

We investigated the possibility that SHOU4 proteins directly interact with CESAs. Using a yeast two-hybrid assay, we found that the intracellular N-terminal domains of SHOU4/4L interacted strongly with the central cytoplasmic domain of CESA1 and weakly with CESA3, but not appreciably with CESA6 (Figures 4E and S4J). The CESA1 interaction was corroborated using a co-immunoprecipitation assay (Figure 4F). Based on these results, we hypothesized that the interaction between SHOU4 and CESA may define the rate of CESA exocytosis and that the levels of SHOU4 proteins play a central role in regulating this process. Consistent with this, a subset of lines overexpressing *SHOU4* from its own promoter (*SHOU4::SHOU4*) displayed root tip swelling and reduced root elongation when grown in the presence of 4.5% sucrose (Figures 4G and 4H), correlating with the levels of *SHOU4* overexpression (Figure 4I). This result, combined with the haploinsufficiency of *SHOU4*, indicates that the stoichiometry of the SHOU4-CESA complex might define the level of CESA exocytosis.

DISCUSSION

Here, we describe a group of novel plant-specific proteins that regulate the level of CESA complexes at the cell surface by modulating the rate of CESA exocytosis. Disruption of *SHOU4* and *SHOU4L* leads to severe pleiotropic defects, suggesting that they regulate cellulose biosynthesis throughout plant growth and development. The elevated CESA complex density at the cell surface in the double *shou4-3 shou4l-1* mutants and the resultant increase in the rate of cellulose synthesis explain the *shou4*-mediated suppression of the cell expansion defects of cellulose-deficient mutants, such as *fei1 fei2*, *sos5*, or prc^{cesa6}. Likewise, the suppression of *shou4-3 shou4l-1* dwarf phenotype by *fei1 fei2* is likely a consequence of cellulose levels being reduced by the *fei* mutations back to a level that is compatible with optimal growth and development. Similarly, our data indicate that inhibition of cellulose biosynthesis through application of isoxaben facilitates the re-emergence of root hairs in *shou4-3 shou4l-1* mutants. This suggests that the increased level of cellulose in *shou4-3 shou4l-1* inhibits the emergence of root hairs, likely by rendering the localized loosening of the wall insufficient

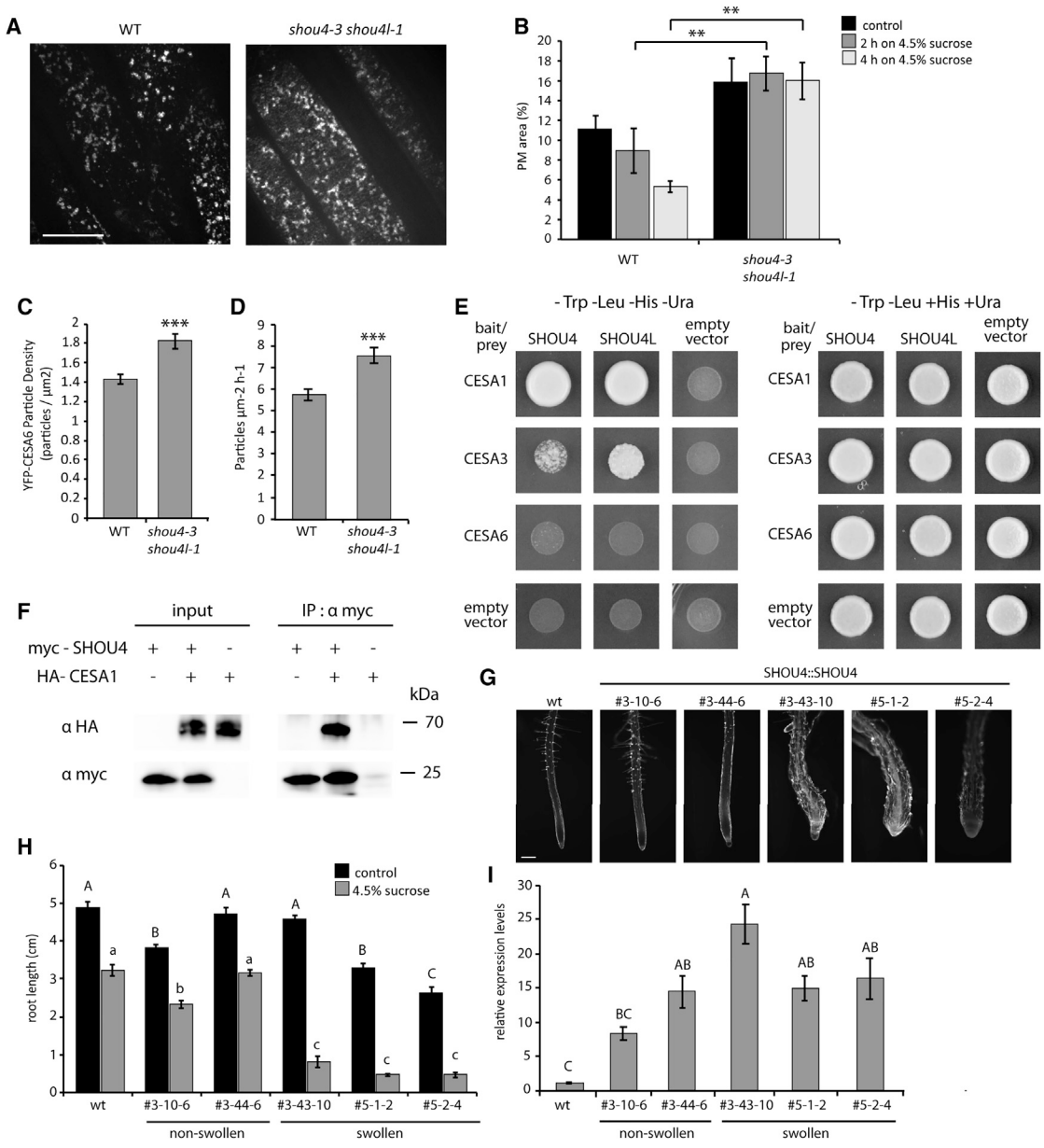

Figure 4. *shou4 shou4l* Mutants Have Increased Density of PM-Localized CESA6-YFP due to Enhanced Exocytosis

SHOU4/4L interact with primary wall CESAs, and *SHOU4* overexpression leads to reduction in root elongation and cell swelling. See also Figure S4 and Videos S1 and S2.

(A) Spinning disk confocal micrographs of CESA6-YFP and CESA6-YFP *shou4-3 shou4l-1* root epidermal cells after 2 hr on media containing 4.5% sucrose. The scale bar represents 20 µm.

(B) Quantification of PM-localized CESA6-YFP signal in different treatments shown in (A). Particles were quantified by measuring thresholded area of the PM; n > 15. See STAR Methods for additional details.

(C) Quantification of CESA6-YFP particle density in epidermal cells of three-day-old etiolated hypocotyls; n ≥ 15 cells from different seedlings per genotype.

(D) CESA6-YFP delivery rate to the PM of epidermal cells is increased in the *shou4-3 shou4l-1* mutant. Fluorescent recovery after photobleaching (FRAP) analysis of CESA6-YFP in WT and *shou4-3 shou4l-1* etiolated hypocotyls; n = 9 cells from different seedlings per genotype.

(E) Yeast two-hybrid assay of interactions between the N-terminal domains of SHOU4/4L proteins and central domains of CESA1, 3, and 6. Seven microliters of a cell suspension was spotted on selection (−Trp −Leu −His −Ura) and control (−Trp −Leu +His +Ura) media. The empty bait and prey vectors were used as negative controls.

(F) N-terminal domain of SHOU4 interacts with the intracellular loop of CESA1 as shown by a co-immunoprecipitation assay. *Nicotiana benthamiana* leaves were transiently transformed with plasmids expressing myc-SHOU4 and HA-CESA1. Total protein extracts (input) and the immunoprecipitated (IP: α-myc) proteins were analyzed by immunoblotting with the indicated antibodies.

(G–I) Overexpression of *SHOU4* can lead to root tip swelling (G) and inhibition of root elongation (H) on media containing 4.5% sucrose.

(G) Root tips of 10-day-old seedlings; scale bar, 250 µm.

(legend continued on next page)

for turgor pressure to push out the emergent hairs in the trichoblast cells. Consistent with this, mutants with reduced levels of cellulose, such as *prc1*, can display bulging trichoblasts or develop extra root hairs [28].

The enhanced density of CESA complexes at the PM in *shou4-3 shou4l-1* seedlings, surprisingly, does not lead to an increase in the levels of crystalline cellulose but rather an increase in amorphous cellulose. The higher number of CESA particles at the cell surface might lead to non-optimal synthesis of cellulose, perhaps due to an inability to channel-sufficient substrate to an increased number of active CESA complexes or to insufficiency of another component involved in cellulose synthesis, such as KORRIGAN [29]. A recently developed model suggests that newly formed cellulose protofibrils go through a temporary disorganized stage before subsequent crystallization [30]. Thus, the increased density of CESA complexes in the *shou4-3 shou4l-1* double mutant might lead to entanglement of the newly synthesized polymers, delaying crystallization of the microfibrils.

Several elements involved in CESA trafficking have been identified. Recent studies have highlighted the importance of efficient clathrin-mediated endocytosis of CSCs and the role of TWD40-2 and AP2M proteins in this process [31, 32]. The *ap2m-1* ($\mu 2$) mutant, which is compromised in endocytosis, displays increased density of PM-localized CESA6-YFP particles, indicating that mis-regulation of trafficking can increase the density of CESAs at the cell surface [31, 33, 34]. The *twd40-2* mutant also has elevated PM-localized CESA6-YFP but, unlike the *apm2* mutant, has reduced levels of crystalline cellulose. TWD40-2, together with AP2M, might remove faulty CSCs from the PM. The reduced crystalline cellulose content in *twd40-2/twd40-2 ap2m* mutants has been hypothesized to result from an inability to internalize catalytically inactive CESAs [32].

Regulation of CSC exocytosis has not been well studied. Recent findings indicate a role for the V-ATPase and STELLO (STL) proteins in CSC assembly and exocytosis [33, 34], but the mechanism involved in the fusion of CSC-containing vesicles with the PM is unknown. *stl1 stl2* double mutants have reduced CSC insertion rates at the PM. Interestingly, despite the superficial resemblance of *shou4-3 shou4l-1* and *stl1 stl2* mutants (both are dwarf with thinner cell walls), there are multiple contrasting phenotypes, including the levels of cellulose in the seed mucilage and sensitivity to isoxaben. A recent study highlights a new role of the CESA- and CSI1-interacting protein PATROL1 (PTL1) in assisting the delivery of CESAs to the PM [35]. To our knowledge, SHOU4 and SHOU4L are the first proteins shown to negatively regulate CSC exocytosis. We demonstrate that the cytoplasmic domains of SHOU4 and SHOU4L interact with the central domain of primary CESAs; however, the mechanism by which the SHOU4 proteins inhibit the exocytosis of CESA complexes remains an open question. The haploinsufficiency of *SHOU4* and the negative effect of even modest SHOU4 overexpression on proper root elongation suggest that the level of the SHOU4 proteins is critical to their function. We favor a model in which the interaction of CESA and SHOU4 generates a signal that feedbacks to negatively regulate CESA exocytosis. Such a "counting" model is consistent with the sensitivity of the system to SHOU4 protein levels. Alternatively, SHOU4/4L might act directly by interacting with the exocytotic machinery at the PM to inhibit delivery of CESA particles.

Our studies have uncovered a novel protein family that interacts with CESAs and regulates their exocytosis, thereby ensuring the optimal abundance of CESA complexes at the PM. Disruption of the *SHOU4* genes leads to multiple defects throughout development, likely as a result of overproduction of cellulose that interferes with the regulation of cell expansion in multiple contexts. These results highlight the importance of CESA trafficking as a critical mechanism to regulate cellulose synthesis to facilitate the dynamic regulation of wall synthesis during multiple developmental processes.

STAR★METHODS

Detailed methods are provided in the online version of this paper and include the following:

- KEY RESOURCES TABLE
- CONTACT FOR REAGENT AND RESOURCE SHARING
- EXPERIMENTAL MODEL AND SUBJECT DETAILS
- METHOD DETAILS
  - Plant growth and generation of constructs
  - Mapping of *shou4-1*
  - Protein alignment and phylogenetic tree
  - Calcofluor and Pontamine S4B mucilage staining
  - Light, confocal laser scanning and transmission electron microscopy
  - Immunogold labeling
  - mRNA transcript and protein levels
  - Yeast two-hybrid and co-immunoprecipitation assays
  - Analysis of *Arabidopsis* cell wall polysaccharides
- QUANTIFICATION AND STATISTICAL ANALYSIS

SUPPLEMENTAL INFORMATION

Supplemental Information includes four figures, two tables, and two videos and can be found with this article online at https://doi.org/10.1016/j.cub.2018.07.076.

ACKNOWLEDGMENTS

The authors thank Victoria Madden, Kristen White, Tony Perdue, and Jamie Winshell for valuable assistance. This work has been supported by grant IOS 1456658 from the National Science Foundation to J.J.K.; Rubicon grant 825.13.018 of the Netherlands Organisation for Scientific Research (NWO) to J.K.P.; the Center for Lignocellulose Structure and Formation, an Energy Frontier Research Center funded by DOE, Office of Science, BES under award no.

(H) Quantification of root elongation of seedlings grown on control and 4.5% sucrose media for 10 days.

(I) *SHOU4* mRNA transcript quantification of the lines shown in (G) and (H) using the $2^{-\Delta\Delta CT}$ method [26]; n = 3 or 4 biological replicates. (B), (C), (D), (H), and (I) are means ± SEM.

Data were analyzed by unpaired Student's t test (B–D; asterisks indicate significant differences relative to the WT; $^{**}p < 0.01$; $^{***}p < 0.001$) and one-way ANOVA and Tukey-Kramer post hoc comparisons (H and I); $p < 0.05$.

DE-SC0001090 to W.J.B., J.L.H., M.T., and C.T.A.; and the Cluster of Excellence on Plant Science (CEPLAS) to C.V. and M.P.

AUTHOR CONTRIBUTIONS

J.J.K. and J.K.P. designed research; J.K.P., W.J.B., C.V., S.D., and B.S. performed experiments and analyzed data; J.L.H. and M.T. provided materials and technical assistance; and J.J.K., C.T.A., and M.P. supervised the project. J.K.P., W.J.B., C.V., J.L.H., J.J.K., C.T.A., and M.P. wrote the manuscript.

DECLARATION OF INTERESTS

The authors declare no competing interests.

Received: January 8, 2018
Revised: June 28, 2018
Accepted: July 27, 2018
Published: September 20, 2018

REFERENCES

1. Kesten, C., Menna, A., and Sánchez-Rodríguez, C. (2017). Regulation of cellulose synthesis in response to stress. Curr. Opin. Plant Biol. *40*, 106–113.
2. McFarlane, H.E., Döring, A., and Persson, S. (2014). The cell biology of cellulose synthesis. Annu. Rev. Plant Biol. *65*, 69–94.
3. Wolf, S. (2017). Plant cell wall signalling and receptor-like kinases. Biochem. J. *474*, 471–492.
4. Xu, S.L., Rahman, A., Baskin, T.I., and Kieber, J.J. (2008). Two leucine-rich repeat receptor kinases mediate signaling, linking cell wall biosynthesis and ACC synthase in *Arabidopsis*. Plant Cell *20*, 3065–3079.
5. Harpaz-Saad, S., McFarlane, H.E., Xu, S., Divi, U.K., Forward, B., Western, T.L., and Kieber, J.J. (2011). Cellulose synthesis via the FEI2 RLK/SOS5 pathway and cellulose synthase 5 is required for the structure of seed coat mucilage in Arabidopsis. Plant J. *68*, 941–953.
6. Fagard, M., Desnos, T., Desprez, T., Goubet, F., Refregier, G., Mouille, G., McCann, M., Rayon, C., Vernhettes, S., and Höfte, H. (2000). *PROCUSTE1* encodes a cellulose synthase required for normal cell elongation specifically in roots and dark-grown hypocotyls of Arabidopsis. Plant Cell *12*, 2409–2424.
7. Shi, H., Kim, Y., Guo, Y., Stevenson, B., and Zhu, J.-K. (2003). The *Arabidopsis SOS5* locus encodes a putative cell surface adhesion protein and is required for normal cell expansion. Plant Cell *15*, 19–32.
8. Schindelman, G., Morikami, A., Jung, J., Baskin, T.I., Carpita, N.C., Derbyshire, P., McCann, M.C., and Benfey, P.N. (2001). *COBRA* encodes a putative GPI-anchored protein, which is polarly localized and necessary for oriented cell expansion in *Arabidopsis*. Genes Dev. *15*, 1115–1127.
9. Chang, J.-M., Di Tommaso, P., Taly, J.-F., and Notredame, C. (2012). Accurate multiple sequence alignment of transmembrane proteins with PSI-Coffee. BMC Bioinformatics *13* (*Suppl 4*), S1.
10. Omasits, U., Ahrens, C.H., Müller, S., and Wollscheid, B. (2014). Protter: interactive protein feature visualization and integration with experimental proteomic data. Bioinformatics *30*, 884–886.
11. Lang, I., Barton, D.A., and Overall, R.L. (2004). Membrane-wall attachments in plasmolysed plant cells. Protoplasma *224*, 231–243.
12. Heim, D.R., Roberts, J.L., Pike, P.D., and Larrinua, I.M. (1990). A second locus, *ixr B1* in *Arabidopsis thaliana*, that confers resistance to the herbicide isoxaben. Plant Physiol. *92*, 858–861.
13. Gutierrez, R., Lindeboom, J.J., Paredez, A.R., Emons, A.M.C., and Ehrhardt, D.W. (2009). *Arabidopsis* cortical microtubules position cellulose synthase delivery to the plasma membrane and interact with cellulose synthase trafficking compartments. Nat. Cell Biol. *11*, 797–806.
14. Crowell, E.F., Bischoff, V., Desprez, T., Rolland, A., Stierhof, Y.-D., Schumacher, K., Gonneau, M., Höfte, H., and Vernhettes, S. (2009). Pausing of Golgi bodies on microtubules regulates secretion of cellulose synthase complexes in *Arabidopsis*. Plant Cell *21*, 1141–1154.
15. Lei, L., Singh, A., Bashline, L., Li, S., Yingling, Y.G., and Gu, Y. (2015). CELLULOSE SYNTHASE INTERACTIVE1 is required for fast recycling of cellulose synthase complexes to the plasma membrane in *Arabidopsis*. Plant Cell *27*, 2926–2940.
16. Bibikova, T.N., Jacob, T., Dahse, I., and Gilroy, S. (1998). Localized changes in apoplastic and cytoplasmic pH are associated with root hair development in *Arabidopsis thaliana*. Development *125*, 2925–2934.
17. Cho, H.T., and Cosgrove, D.J. (2002). Regulation of root hair initiation and expansin gene expression in *Arabidopsis*. Plant Cell *14*, 3237–3253.
18. Voiniciuc, C., Yang, B., Schmidt, M.H., Günl, M., and Usadel, B. (2015). Starting to gel: how *Arabidopsis* seed coat epidermal cells produce specialized secondary cell walls. Int. J. Mol. Sci. *16*, 3452–3473.
19. Anderson, C.T., Carroll, A., Akhmetova, L., and Somerville, C. (2010). Real-time imaging of cellulose reorientation during cell wall expansion in *Arabidopsis* roots. Plant Physiol. *152*, 787–796.
20. Ben-Tov, D., Abraham, Y., Stav, S., Thompson, K., Loraine, A., Elbaum, R., de Souza, A., Pauly, M., Kieber, J.J., and Harpaz-Saad, S. (2015). COBRA-LIKE2, a member of the glycosylphosphatidylinositol-anchored COBRA-LIKE family, plays a role in cellulose deposition in *arabidopsis* seed coat mucilage secretory cells. Plant Physiol. *167*, 711–724.
21. Updegraff, D.M. (1969). Semimicro determination of cellulose in biological materials. Anal. Biochem. *32*, 420–424.
22. Boraston, A.B., Chiu, P., Warren, R.A., and Kilburn, D.G. (2000). Specificity and affinity of substrate binding by a family 17 carbohydrate-binding module from *Clostridium cellulovoran*s cellulase 5A. Biochemistry *39*, 11129–11136.
23. Blake, A.W., McCartney, L., Flint, J.E., Bolam, D.N., Boraston, A.B., Gilbert, H.J., and Knox, J.P. (2006). Understanding the biological rationale for the diversity of cellulose-directed carbohydrate-binding modules in prokaryotic enzymes. J. Biol. Chem. *281*, 29321–29329.
24. Ruel, K., Nishiyama, Y., and Joseleau, J.P. (2012). Crystalline and amorphous cellulose in the secondary cell walls of Arabidopsis. Plant Sci. *193-194*, 48–61.
25. Paredez, A.R., Somerville, C.R., and Ehrhardt, D.W. (2006). Visualization of cellulose synthase demonstrates functional association with microtubules. Science *312*, 1491–1495.
26. Livak, K.J., and Schmittgen, T.D. (2001). Analysis of relative gene expression data using real-time quantitative PCR and the 2(-Δ Δ C(T)) method. Methods *25*, 402–408.
27. Sampathkumar, A., Gutierrez, R., McFarlane, H.E., Bringmann, M., Lindeboom, J., Emons, A.-M., Samuels, L., Ketelaar, T., Ehrhardt, D.W., and Persson, S. (2013). Patterning and lifetime of plasma membrane-localized cellulose synthase is dependent on actin organization in *Arabidopsis* interphase cells. Plant Physiol. *162*, 675–688.
28. Singh, S.K., Fischer, U., Singh, M., Grebe, M., and Marchant, A. (2008). Insight into the early steps of root hair formation revealed by the *procuste1* cellulose synthase mutant of *Arabidopsis thaliana*. BMC Plant Biol. *8*, 57.
29. Nicol, F., His, I., Jauneau, A., Vernhettes, S., Canut, H., and Höfte, H. (1998). A plasma membrane-bound putative endo-1,4-beta-D-glucanase is required for normal wall assembly and cell elongation in *Arabidopsis*. EMBO J. *17*, 5563–5576.
30. Haigler, C.H., Grimson, M.J., Gervais, J., Le Moigne, N., Höfte, H., Monasse, B., and Navard, P. (2014). Molecular modeling and imaging of initial stages of cellulose fibril assembly: evidence for a disordered intermediate stage. PLoS ONE *9*, e93981.
31. Bashline, L., Li, S., Anderson, C.T., Lei, L., and Gu, Y. (2013). The endocytosis of cellulose synthase in Arabidopsis is dependent on μ2, a clathrin-mediated endocytosis adaptin. Plant Physiol. *163*, 150–160.
32. Bashline, L., Li, S., Zhu, X., and Gu, Y. (2015). The TWD40-2 protein and the AP2 complex cooperate in the clathrin-mediated endocytosis of cellulose synthase to regulate cellulose biosynthesis. Proc. Natl. Acad. Sci. USA *112*, 12870–12875.

33. Luo, Y., Scholl, S., Doering, A., Zhang, Y., Irani, N.G., Rubbo, S.D., Neumetzler, L., Krishnamoorthy, P., Van Houtte, I., Mylle, E., et al. (2015). V-ATPase activity in the TGN/EE is required for exocytosis and recycling in Arabidopsis. Nat. Plants *1*, 15094.

34. Zhang, Y., Nikolovski, N., Sorieul, M., Vellosillo, T., McFarlane, H.E., Dupree, R., Kesten, C., Schneider, R., Driemeier, C., Lathe, R., et al. (2016). Golgi-localized STELLO proteins regulate the assembly and trafficking of cellulose synthase complexes in *Arabidopsis*. Nat. Commun. *7*, 11656.

35. Zhu, X., Li, S., Pan, S., Xin, X., and Gu, Y. (2018). CSI1, PATROL1, and exocyst complex cooperate in delivery of cellulose synthase complexes to the plasma membrane. Proc. Natl. Acad. Sci. USA *115*, E3578–E3587.

36. Hill, J.L., Jr., Josephs, C., Barnes, W.J., Anderson, C.T., and Tien, M. (2018). Longevity in vivo of primary cell wall cellulose synthases. Plant Mol. Biol. *96*, 279–289.

37. Dortay, H., Mehnert, N., Bürkle, L., Schmülling, T., and Heyl, A. (2006). Analysis of protein interactions within the cytokinin-signaling pathway of *Arabidopsis thaliana*. FEBS J. *273*, 4631–4644.

38. Steinwand, B.J., Xu, S., Polko, J.K., Doctor, S.M., Westafer, M., and Kieber, J.J. (2014). Alterations in auxin homeostasis suppress defects in cell wall function. PLoS ONE *9*, e98193.

39. Benková, E., Michniewicz, M., Sauer, M., Teichmann, T., Seifertová, D., Jürgens, G., and Friml, J. (2003). Local, efflux-dependent auxin gradients as a common module for plant organ formation. Cell *115*, 591–602.

40. Nakagawa, T., Kurose, T., Hino, T., Tanaka, K., Kawamukai, M., Niwa, Y., Toyooka, K., Matsuoka, K., Jinbo, T., and Kimura, T. (2007). Development of series of gateway binary vectors, pGWBs, for realizing efficient construction of fusion genes for plant transformation. J. Biosci. Bioeng. *104*, 34–41.

41. Earley, K.W., Haag, J.R., Pontes, O., Opper, K., Juehne, T., Song, K., and Pikaard, C.S. (2006). Gateway-compatible vectors for plant functional genomics and proteomics. Plant J. *45*, 616–629.

42. Tamura, K., Stecher, G., Peterson, D., Filipski, A., and Kumar, S. (2013). MEGA6: molecular evolutionary genetics analysis version 6.0. Mol. Biol. Evol. *30*, 2725–2729.

43. Schindelin, J., Arganda-Carreras, I., Frise, E., Kaynig, V., Longair, M., Pietzsch, T., Preibisch, S., Rueden, C., Saalfeld, S., Schmid, B., et al. (2012). Fiji: an open-source platform for biological-image analysis. Nat. Methods *9*, 676–682.

44. Rapsomaniki, M.A., Kotsantis, P., Symeonidou, I.E., Giakoumakis, N.N., Taraviras, S., and Lygerou, Z. (2012). easyFRAP: an interactive, easy-to-use tool for qualitative and quantitative analysis of FRAP data. Bioinformatics *28*, 1800–1801.

45. Alonso, J.M., Stepanova, A.N., Leisse, T.J., Kim, C.J., Chen, H., Shinn, P., Stevenson, D.K., Zimmerman, J., Barajas, P., Cheuk, R., et al. (2003). Genome-wide insertional mutagenesis of *Arabidopsis thaliana*. Science *301*, 653–657.

46. Neff, M.M., Neff, J.D., Chory, J., and Pepper, A.E. (1998). dCAPS, a simple technique for the genetic analysis of single nucleotide polymorphisms: experimental applications in *Arabidopsis thaliana* genetics. Plant J. *14*, 387–392.

47. Austin, R.S., Vidaurre, D., Stamatiou, G., Breit, R., Provart, N.J., Bonetta, D., Zhang, J., Fung, P., Gong, Y., Wang, P.W., et al. (2011). Next-generation mapping of *Arabidopsis* genes. Plant J. *67*, 715–725.

48. Sessions, A., Weigel, D., and Yanofsky, M.F. (1999). The *Arabidopsis thaliana* MERISTEM LAYER 1 promoter specifies epidermal expression in meristems and young primordia. Plant J. *20*, 259–263.

49. Schenk, S.T., and Schikora, A. (2015). Staining of callose depositions in root and leaf tissues. Bio-protocol *5*, e1429.

50. Wang, W., Vignani, R., Scali, M., and Cresti, M. (2006). A universal and rapid protocol for protein extraction from recalcitrant plant tissues for proteomic analysis. Electrophoresis *27*, 2782–2786.

51. Hill, J.L., Jr., Hammudi, M.B., and Tien, M. (2014). The *Arabidopsis* cellulose synthase complex: a proposed hexamer of CESA trimers in an equimolar stoichiometry. Plant Cell *26*, 4834–4842.

52. Shanks, C.M., Hecker, A., Cheng, C.-Y., Brand, L., Collani, S., Schmid, M., Schaller, G.E., Wanke, D., Harter, K., and Kieber, J.J. (2018). Role of BASIC PENTACYSTEINE transcription factors in a subset of cytokinin signaling responses. Plant J. *95*, 458–473.

53. Gietz, R.D., and Schiestl, R.H. (2007). High-efficiency yeast transformation using the LiAc/SS carrier DNA/PEG method. Nat. Protoc. *2*, 31–34.

54. Fuxman Bass, J.I., Reece-Hoyes, J.S., and Walhout, A.J.M. (2016). Colony lift colorimetric assay for β-galactosidase activity. Cold Spring Harb. Protoc. *2016*, pdb.prot088963.

55. Yang, Y., Li, R., and Qi, M. (2000). In vivo analysis of plant promoters and transcription factors by agroinfiltration of tobacco leaves. Plant J. *22*, 543–551.

56. Foster, C.E., Martin, T.M., and Pauly, M. (2010). Comprehensive compositional analysis of plant cell walls (lignocellulosic biomass) part II: carbohydrates. J. Vis. Exp. (37), 1837.

57. Voiniciuc, C., and Günl, M. (2016). Analysis of monosaccharides in total mucilage extractable from *Arabidopsis* seeds. Bio-protocol. *6*, e1801.

58. Voiniciuc, C., Schmidt, M.H.W., Berger, A., Yang, B., Ebert, B., Scheller, H.V., North, H.M., Usadel, B., and Günl, M. (2015). MUCILAGE-RELATED10 produces galactoglucomannan that maintains pectin and cellulose architecture in Arabidopsis seed mucilage. Plant Physiol. *169*, 403–420.

59. McCloy, R.A., Rogers, S., Caldon, C.E., Lorca, T., Castro, A., and Burgess, A. (2014). Partial inhibition of Cdk1 in G 2 phase overrides the SAC and decouples mitotic events. Cell Cycle *13*, 1400–1412.

60. Walser, M., Hajnal, A., and Escobar-Restrepo, J.M. (2015). FRAP analysis of LET-23:GFP in the vulval epithelial cells of living *Caenorhabditis elegans* larvae. Bio-protocol *5*, e1489.

STAR★METHODS

KEY RESOURCES TABLE

REAGENT or RESOURCE	SOURCE	IDENTIFIER
Antibodies		
rabbit anti-HIS	Sigma	SAB1306085
anti-CESA1	[36]	N/A
anti-CESA3	[36]	N/A
anti-CESA6	[36]	N/A
rabbit anti-tubulin	Sigma	SAB3501071; RRID: AB_2713894
goat anti-Rabbit IgG (H+L) Antibody, Peroxidase labeled	KPL	95058
rat anti-HA	Roche	11867423001; RRID: AB_390918
goat anti-rat IgG–HRP	Santa Cruz Biotechnology	sc-2006; RRID: AB_1125219
mouse anti-c-myc	Santa Cruz Biotechnology	sc-40; RRID: AB_627268
chicken anti-mouse IgG-HRP	Santa Cruz Biotechnology	sc-2954; RRID: AB_639239
Bacterial and Virus Strains		
DH5α	Thermo Fisher Scientific	18265017
GV3101	N/A	N/A
Chemicals, Peptides, and Recombinant Proteins		
phytagel	Sigma	P8169
isoxaben	Santa Cruz Biotechnology	sc-235431
Murashige and Skoog (MS) salts	Research Products International	M70300-50.0
Calcofluor fluorescent brightener 28	Sigma	F3543-1g
Pontamine Fast Scarlet S4B	Sigma	S479896
X-Gluc	Goldbio	114162-64-0
Aniline blue	Fisher Scientific	A-967
CBM28	Dr. Paul Knox	N/A
Gold-conjugated protein A	Ted Pella	15822
Fish gelatin	Sigma	G7765
α-amylase	Sigma Aldrich	A3403-500KU
pullulanase	Sigma Aldrich	E2412-50ml
Critical Commercial Assays		
RNeasy Mini kit	QIAGEN	74104
Protoscript II cDNA synthesis kit	New England Biolabs	E6560S
PowerUp SYBR Green Master Mix	Life Technologies	A25742
Pierce BCA Protein Assay Kit	Fisher Scientific	23227
μMACS c-myc Isolation Kit	Miltenyi Biotec	130-091-123
cOmplete ULTRA Tablets, Mini, EDTA-free, *EASYpack* Protease Inhibitor Cocktail	Roche	5892791001
SuperSignal West Femto Maximum Intensity Substrate	Thermo Fisher Scientific	34095
Experimental Models: Cell Lines		
L40ccαU yeast strain	[37]	N/A
Experimental Models: Organisms/Strains		
WT (Col-0)	ABRC	N/A
shou4-3	ABRC	GK793F10
shou4l-1	ABRC	SALK_001751
shou4l-2	ABRC	SALK_205329
shou4l2-1	ABRC	SALK_029810
fei1 fei2	[4]	N/A

(*Continued on next page*)

Continued

REAGENT or RESOURCE	SOURCE	IDENTIFIER
fei1 fei2 in L*er*	[38]	N/A
sos5-2	[7]	N/A
cob-1	[8]	N/A
CESA6-YFP	[25]	N/A
PIN1-GFP	[39]	N/A
prc-1	[6]	N/A
SHOU4::SHOU4:GFP in WT	this study	N/A
SHOU4::SHOU4:mCherry in WT	this study	N/A
SHOU4::SHOU4:GFP in *fei1 fei2 shou4-1*	this study	N/A
SHOU4::SHOU4:mCherry in *fei1 fei2 shou4-1*	this study	N/A
SHOU4::GUS in WT	this study	N/A
Oligonucleotides		
primers	Please see Table S1	N/A
Recombinant DNA		
pGWB3	[40]	N/A
pGWB4	[40]	N/A
modified pGWB4 (mCherry)	This study	N/A
pENTR-dTOPO	Invitrogen	K2400-20
pBTMN116c-D9	[37]	N/A
pACT2	[37]	N/A
pEarleyGate201	[41]	N/A
pEarleyGate203	[41]	N/A
SHOU4-pBTMN116	This study	N/A
SHOU4L-pBTMN116	This study	N/A
CESA1-pACT2	This study	N/A
CESA3-pACT2	This study	N/A
CESA6-pACT2	This study	N/A
myc-SHOU4	This study	N/A
HA-CESA1	This study	N/A
Software and Algorithms		
PSI/TM Coffee	[9]	N/A
MEGA6	[42]	N/A
ImageJ	[43]	N/A
Imaris	Bitplane	N/A
EasyFRAP	[44]	N/A
AutoQuant X2	Media cybernetics	N/A
Other		
Confocal microscopes and image aqusition settings	Please see Table S2	N/A

CONTACT FOR REAGENT AND RESOURCE SHARING

Further information and requests for resources and reagents should be directed to and will be fulfilled by the Lead Contact, Joseph J. Kieber (jkieber@unc.edu).

EXPERIMENTAL MODEL AND SUBJECT DETAILS

The WT Columbia-0 (Col-0) was use in all experiments. The T-DNA insertional alleles *shou4-3* (GK793F10), *shou4l-1* (SALK_001751), *shou4l-2* (SALK_205329) and *shou4l2-1* (SALK_029810) were obtained from the SALK T-DNA collection [45]. The *fei1*, *fei2* [4], *sos5-2* [7] *prc-1*^{cesa6} [6], *cob-1* [8], CESA6-YFP [25], PIN1-GFP [39] alleles have been previously described. Plants were genotyped using primers listed in Table S1. The *prc-1*, *cob-1* and *shou4-1* were genotyped using a dCAPS method [46].

METHOD DETAILS

Plant growth and generation of constructs

For root elongation assays, seeds were surface-sterilized, plated on media containing 1 x Murashige and Skoog (MS) salts (Research Products International), 0.6% phytagel (Sigma, St Louis, MO, USA) and either 0% or 4.5% sucrose, stratified for 2-4 days at 4°C and subsequently grown at 22°C under constant light. When specified, seedlings were first grown for 4 days and then transferred onto media containing either 0% or 4.5% sucrose. For etiolated hypocotyl experiments, seeds were plated on media containing 1% sucrose, stratified for 3 days, exposed to light for 3 h and subsequently grown in the dark at 22°C for 3 days. For isoxaben treatment of roots, seedlings were first grown on media containing no sucrose and at 4 days post germination transferred onto media with a 0.1% ethanol (vehicle control), 1 nM or 2 nM isoxaben (Santa Cruz Biotechnology) for 18-24 hours. Root width measurements were performed at the level of the youngest root hair and hypocotyl width measurements were conducted just below the apical hook. For the isoxaben treatment of 3d-old etiolated CESA6-YFP; SHOU4-mCherry hypocotyls, seedlings were incubated for 3 hours in MS media containing 200 nM isoxaben in dark with gentle shaking.

The *SHOU4* translational fusions with GFP/mCherry were created by amplifying the promoter and genomic sequence of At1g78880 and cloning it first into pENTR/dTOPO and subsequently into the pGWB4 binary vector [40] or a modified (mCherry) version of pGWB4. The *SHOU4::GUS* promoter fusions were created by amplifying the 627 bp sequence upstream of At1g78880 and cloning it into the pGWB3 binary vector [40]. The Y2H and coIP constructs were generated in a similar manner. First, the sequences of the appropriate domains of *SHOU4*, *SHOU4L*, *CESA1*, *CESA3* and *CESA6* were cloned into the pENTR/dTOPO (Primers are listed in Table S1). Subsequently, they were cloned into the binary vectors (Y2H; bait - pBMTN116c-D9 and prey- pACT2; coIP - pEarleyGate201/203 (pEG201 and pEG203)) have previously been described [37, 41]. Note all constructs were verified by sequencing.

To study the nature of *shou4-1* mutation, we transformed WT and *fei1 fei2 shou4-1* plants with the WT sequence of the *SHOU4*::*SHOU4*:GFP/mCherry. Homozygous T3 progeny of T2 plants that segregated for the transgene in a 3:1 ratio (transgenic:WT) were used. For the GUS assay, T2 seedling from five independent transformation events were stained and representative individuals were chosen for imaging. To create a CESA6-YFP; SHOU4-mCherry double transgenic line, we transformed CESA6-YFP plants with the *SHOU4::SHOU4:mCherry* construct and imaged T2 seedlings. We chose individuals that displayed fluorescence of both YFP and mCherry proteins.

Mapping of *shou4-1*

To identify *shou4-1,* we used the Next Generation Mapping tool [47]. The *fei1 fei2* mutations (Columbia-0, Col-0 ecotype) were introgressed into Landsberg *erecta* (L*er*) ecotype as described by Steinwand et al. [38]. The *fei1 fei2 shou4-1* (Col-0) triple mutant was outcrossed to the *fei1 fei2* (L*er*) mutant and the phenotype of the individuals from the F2 progeny was scored. DNA pools containing WT or mutant DNA were subjected to Illumina sequencing and the data then analyzed using the Next Generation Mapping (NGM) tool [47], which bins and plots SNP frequencies in 250 kb intervals across the *Arabidopisis* genome. Regions lacking in SNPs correspond to non-recombinant blocks created by linkage to the causative mutation [47]. The background *fei1* and *fei2* mutations, which are T-DNA insertion alleles, localize to the upper arm of chromosome 1 and the lower arm of chromosome 2, respectively [4] and, since they created non-recombinant blocks in the genome, were identified in the SNP plots created using NGM (Figure S1B). An additional non-recombinant region was identified near the end of chromosome 1 (Figure S1B). We analyzed differential SNPs in this non-recombinant region in reference to the annotated genome. NGM uses a 'discordant chastity' (Ch_D) value to quantify the proportion of reads at a polymorphic site that differ from the reference genome. We set the Ch_D to 0.8 and identified a G/C→A/T transition in At1g78880 (Figure 1C). Sanger sequencing of AT1G78880 in both the *fei1 fei2* parent and in the *fei1 fei2 shou4-1* suppressor confirmed the presence of the G/C→T/A substitution. Consistent with the fact that *shou4-1* lies within a splice site, comparison of the sequences of *SHOU4* cDNA from the suppressor and WT revealed alternative splicing of *SHOU4* mRNA in the *fei1 fei2 shou4-1* mutant (Figure 1C).

Protein alignment and phylogenetic tree

SHOU4, SHOU4L and SHOU4L2 protein alignment and prediction of transmembrane domains were generated using the PSI/TM-Coffee package http://tcoffee.crg.cat/apps/tcoffee/do:tmcoffee) [9]. The neighbor-joining phylogenetic tree of SHOU4 homologs was created using the MEGA6 software [42].

Calcofluor and Pontamine S4B mucilage staining

The calcofluor fluorescent brightener 28 (Sigma) staining was performed as described by [5]. Seeds were incubated in 25 mg/ml calcofluor for 30 min, washed in water and observed in Zeiss LSM710 confocal microscope with a 405 nm-laser diode. Pontamine Fast Scarlet S4B (Sigma) was done as described [19]. Seeds were stained for 30 min in 0.01% Pontamine Fast Scarlet S4B (Sigma) in 1 x MS media, washed for 2 hours in water and then visualized using a Zeiss LSM710 confocal microscope equipped with a 561 laser.

Light, confocal laser scanning and transmission electron microscopy

Cross sections of the root elongation zone were prepared and imaged as described [4]. Roots, stigmas and GUS-stained seedlings were imaged using bright field microscopy. Hypocotyls were photographed using a Nikon D7000 camera. SHOU4-GFP,

SHOU4-mCherry, CESA6-YFP, propidium iodide fluorescence were visualized using Zeiss LSM710, LSM880 confocal microscopes with excitation wavelengths and emission spectra listed in in Table S2.

Imaging experiments for determination of YFP-CESA6 density, velocity, trajectory, and delivery rate in etiolated hypocotyls were performed using a Zeiss Axio Observer SD spinning disk confocal microscope with a CSU-X1 spinning disk head (Yokogawa) using a 100X / 1.40 NA oil immersion objective with AxioVision 4.8 software (Carl Zeiss) and a 488 nm excitation laser with a 525 / 50 nm emission filter. For velocity experiments, 3-day-old etiolated seedlings were mounted in 60 μL water between a microscope slide and a 24 × 40 mm #1.5 coverslip (Corning) secured with double-sided tape (3M Permanent), whereas a 2% low-melt agar (Dot Scientific) pad was used to secure etiolated seedlings in a coverslip chamber for delivery experiments. YFP-CESA6 density and velocity data were derived from the same sets of images (5 min time-lapses with 5 s intervals), with density being determined from the first time-point of the time-lapses for individual cells. All images were acquired in the area of etiolated hypocotyls subtending the apical hook.

For PIN1-GFP FRAP experiments, roots of three-day-old seedlings were used. Seedling were grown as described in the previous section. GFP fluorescence in cortical root cells was imaged with ZEISS LSM 880 using the x40 water objective. The frame size was 1024 × 1024 and the speed scan was 8-15 s per frame. The bleaching settings were: 2 pre-bleach and 23 post-bleach images; 40 iterations at the same speed as pre- and post-bleach acquisition. The 488 nm laser power for the pre-bleach, bleach, and post-bleach images was the same (5%). For the TEM sections, 37d-old *Arabidopsis* inflorescence stems grown in short day were immersion-fixed in 2% glutaraldehyde/0.05M sodium phosphate, pH 7.4, and stored for three days at 4°C. After three buffer washes, the samples were post-fixed in 1% osmium tetroxide/0.05M sodium phosphate, pH 7.4, for 1 h followed by 3 washes in deionized water. Roots and stems were dehydrated through a graded series of ethanol (30%, 50%, 75%, 90%, 100% X3) and propylene oxide, infiltrated and embedded in Spurr's epoxy resin (Polysciences, Warrington, PA). Using a diamond knife, 1 μm transverse sections were cut, mounted on slides and stained with 1% toluidine blue and examined by light microscopy to isolate the region of interest. Ultrathin sections (70-80 nm) were cut with a diamond knife and mounted on 200 mesh copper grids followed by staining with 4% aqueous uranyl acetate for 12 minutes and lead citrate for 8 minutes. Samples were visualized with either Zeiss 910 or JEOL 1230 TEM. The plasmolysis experiment on SHOU4-GFP seedlings was done by incubating plants in a 1 x MS solution (control) and 1 x MS solution containing 0.8 M mannitol for 30 min. The GUS assay was performed as described in [48]. 7d-old seedlings were harvested in ice cold 90% acetone, vacuum-infiltrated in acetone for 20 minutes at room temperature, vacuum-infiltrated in a staining solution without X-Gluc (50 mM sodium phosphate buffer pH 7.0, 0.2% Triton X-100, 2 mM potassium ferrocyanide, 2 mM potassium ferricyanide) for 10 minutes and subsequently vacuum-infiltrated in a staining solution containing 2 mM X-Gluc (5-bromo-4-chloro-3-indolyl-beta-D-glucuronic acid, cyclohexylammonium salt; GoldBio) for 20 min and incubated in the staining solution with X-Gluc for 3 h at 37°C. Samples were incubated in a series of ethanol solutions for 40 minutes each (20%, 30%, 50%, FAA (50% ethanol, 5% acetic acid, 3.7% formaldehyde), 70% ethanol) and stored at 4°C. Aniline blue staining for callose was done as described [49]. Leaves of 11d-old seedlings were fixated and de-stained overnight in 1:3 acetic acid/ethanol solution, incubated for 30 min in 150 mM dipotassium phosphate and subsequently incubated for 2 h in 150 mM dipotassium phosphate containing 0.01% aniline blue. Specimens were embedded in 50% glycerol for further analysis with Zeiss LSM880 confocal microscope.

Immunogold labeling

Immunogold labeling of secondary cell walls using the His-tagged CBM28 was done according to a modified protocol [24]. First, we determined the optimal concentration of CBM28 (Plant Probes) and the His antibody (Sigma Aldrich) by analyzing different concentrations of the antibody. Grids with ultrathin sections were hydrated in water, blocked in 5% milk in phosphate buffered saline (PBS) for 30 min, incubated in 200 μg/ml CBM28 in 5% milk in PBS for 1.5 hours, washed 3 times in 5% milk in PBS and incubated overnight in 1:25 anti-His antibody at 4°C. The following day, grids were washed 5 times in PBS, incubated in gold-conjugated protein A (PAG-15; Ted Pella) diluted in PBS/0.1% fish gelatin (Sigma) (1:50) for 1.5 hour at room temperature. Next, grids were rinsed twice in PBS/fish gelatin, 3 times in PBS, fixed in 2% glutaraldehyde in PBS and rinsed 4 times in water. Post-stain was conducted in 4% aqueous uranyl acetate, grids were subsequently rinsed 5 times in water and dried at room temperature. All solutions had been microfiltered and the staining was performed on silicone stain grids (Ted Pella).

mRNA transcript and protein levels

Roots and shoots of nine-day-old seedlings were harvested and snap frozen in liquid nitrogen. RNA was isolated using the RNeasy extraction kit (QIAGEN). 1 μg total RNA was used for cDNA synthesis conducted using the Protoscript II cDNA synthesis kit (New England Biolabs). Real-time reverse transcription PCR was performed using the Applied Biosystems QuantStudio 6Flex system and the PowerUp SYBR® Green Master Mix (Life Technologies). Relative mRNA values were calculated using the $2^{-\Delta\Delta CT}$ method [26] with β-TUBULIN (At5g44340) or GAPDH (At1g16300) as an internal reference gene. Primer sequences are listed in Table S1. For protein extraction, ten-day-old roots and shoots were harvested and ground in liquid nitrogen and the protein was extracted using the published methods [50, 51]. Protein concentrations were assayed using the Pierce BCA Protein Assay Kit (Thermo Fisher Scientific), samples were diluted to 1 μg/ml in SDS loading buffer, aliquoted and stored at −80°C until used. Protein samples were separated on 8% SDS-PAGE gels with a 5% stacking gel (pH 8.8, with 35% glycerol) and transferred onto 0.45 μm pore nitrocellulose blotting membrane (Ge Healthcare Life Science). Blots were blocked in 0.25% Tween-containing Tris-buffered saline (TBS) (TBST), incubated overnight at 4°C with primary CESA antibodies (at concentrations 1:2000, 1:700, 1:1000, 1:5000 for CESA1, CESA3, CESA6 and TUBULIN, respectively), washed in TBST, incubated in a secondary goat anti-rabbit horseradish peroxidase conjugate

(KPL 95058-730) for 1 h at room temperature (at concentrations 1:30000, 1:10000, 1:20000, 1:10000 for CESA1, CESA3, CESA6 and TUBULIN, respectively), washed in TBST and developed using SuperSignal West Femto Maximum Intensity Substrate (Thermo Fisher Scientific). Chemiluminescence was visualize using the ChemiDoc Touch Imaging System (Bio-Rad) and quantified using the Image Lab software relative to the non-specific band (roots) or TUBULIN (Sigma) (shoots). The generation and specificity of Anti-CESA1, CESA3, and CESA were previously describe [36] or affinity purification of antibodies from crude serum, the CESA3-2 or CESA6-1 peptides were conjugated to Sulfo-Link Resin (Thermo) and affinity purification proceeded according to manufacturer's instructions.

Yeast two-hybrid and co-immunoprecipitation assays

The yeast two-hybrid assay was conducted as described previously [52]. Briefly, the L40ccαU strain was transformed by indicated plasmids as described in [53]. Transformants were selected on Leu^- Trp^- media and the presence of plasmids was confirmed by colony PCR. Cell suspensions of transformed yeast were grown overnight and 7 μl of each transformation was spotted on Leu^- Trp^- (control) or Leu^- Trp^- His^- Ura^- media to test the interaction. The X-Gal staining was performed as described by [54] and the yeast colonies were incubated at 37°C for 1h. The GV3101 strain of *Agrobacterium* was transformed with plasmids containing the myc-SHOU4, HA-CESA1 and p19 suppressor. 4-week-old *Nicotiana benthamiana* leaves were infiltrated with the appropriate vectors following the protocol described by [55]. After 48h, the leaves were flash frozen in liquid nitrogen, ground and the coIP was conducted using the μMACS Epitope Tag Protein Isolation Kit (Miltenyi Biotec). Total protein extracts were incubated in cold lysis buffer supplemented with protease inhibitor cocktail, (cOmplete ULTRA Tablets, Mini, EDTA-free, *EASYpack* Protease Inhibitor Cocktail; Roche). The coIP was followed by immunoblotting. Blots were probed with the appropriate antibodies: primary anti-HA high affinity antibody, 3F10, monoclonal (Roche) followed by a secondary antibody goat anti-rat IgG–HRP:sc-2006 (Santa Cruz Biotechnology) for detection of HA and primary c-Myc Antibody (9E10): sc-40 antibody followed by a secondary antibody chicken anti-mouse IgG–HRP: sc2954 (Santa Cruz Biotechnology) for detection of myc. Signal was detected with SuperSignalWest Femto Maximum Sensitivity Substrate (Thermo Fisher Scientific).

Analysis of *Arabidopsis* cell wall polysaccharides

For each genotype, 9 to 16 mg of lyophilized *Arabidopsis* root or shoot material was ground using a steel ball for a total of 2 min at 30 Hz using a ball mill (Retsch MM400). Alcohol-insoluble residue (AIR) was obtained by sequentially washing the ground material once with 1 mL of 70% ethanol, once with 1 mL of chloroform:methanol (1:1 v/v), and once with 1 mL of acetone. After each washing step, the AIR was pelleted by centrifugation (20,000 g for 5 min), and the supernatant was carefully discarded. After the final wash, the pellet was resuspended in 300 μL of acetone, and dried in a fume hood overnight. Crystalline cellulose content in 2 to 3 mg of dry wall AIR was quantified using the Updegraff assay [21], essentially as previously described [56]. Following treatment with the Updegraff reagent, the pellet was washed once with 1.5 mL of water, and once with 1.5 mL of acetone. After each step, the samples were centrifuged for 15 min at 20000*g*, and the supernatant was carefully discarded. After drying the pellet overnight at room temperature, the amount of glucose was analyzed in triplicate with the colorimetric Anthrone assay [56]. *Arabidopsis* shoot samples were de-starched similar to a published protocol [56]. Approximately 2 mg of wall AIR was mixed with a 500 μL of 0.1 M phosphate buffer (pH 7.0) containing 1 μL of thermostable α-Amylase (Sigma Aldrich, A3403-500KU) and 10 μL of Pullulanase (Sigma Aldrich, E2412-50ML). Tubes were incubated at 80°C in a thermomixer (300 rpm) for 30 min, briefly cooled on ice, then mixed horizontally at 225 rpm for 20 h in a 37°C incubator. The undigested material was pelleted (2 min at 20000 g), and washed with twice with 1.5 mL of water, and once with 1.5 mL of acetone before drying. Monosaccharide composition of destarched AIR (1 to 2 mg) was determined using high-performance anion-exchange chromatography with pulsed amperometric detection (HPAEC-PAD), using a published method [57, 58] with minor modifications. After hydrolyzing the material with 1 M trifluoroacetic acid, 150 μL of each supernatant was dried and myo-Inositol was added as an internal standard. Samples were subjected to HPAEC-PAD using a Metrohm system (889 IC Sample Center and 940 Professional IC Vario).

QUANTIFICATION AND STATISTICAL ANALYSIS

Root, hypocotyl length and width measurements, cell size, secondary cell wall thickness and CESA6-YFP particle densities in root epidermal cells were conducted with the FIJI software using a line tool [43]. Cell size and cell wall thickness were measured using the area tool. For the particle density analysis, Z stack images were processed with the maximum intensity projection tool and the detection of PM-localized CESA6-YFP particles was done using threshold function and measuring the thresholded area within a selected ROI. CESA6-YFP density was determined by outlining an individual cell in ImageJ with the polygon selection tool, measuring the area, and detecting YFP-CESA6 particles using the Find Maxima tool with a noise tolerance of 500. Calcoflur and pontamine S4B fluorescence was measured using the FIJI software [43] and the total corrected fluorescence was calculated as described in [59]. Particle speed and trajectories were tracked and quantified using Imaris 7.2 (Bitplane) with an estimated particle diameter of 0.25 μm and a minimum track duration of 30 s. Detected particles with speeds greater than 600 nm/min were excluded from speed analysis because they likely represent YFP-CESA6 signal from intracellular compartments but could not be excluded from trajectory measurements. For determination of YFP-CESA6 delivery rates, ROIs of individual cells were bleached by 100% power 488 nm laser exposure for 4 s,

and recovery of fluorescence was detected via time-lapse imaging (10 min recovery with 10 s intervals). Particle delivery events were assessed following 2D deconvolution specific for YFP emission using the AutoQuantX2 software (Media Cybernetics, Rockville, MD) to allow for differentiation of individual YFP-CESA6 particles in close proximity. Particles were identified manually, and verified for typical CSC motility as previously described [27]. After counting the number of insertion events and determining GFP-CESA3 density within the ROI at 2, 4, 6, 8, and 10 min, a linear regression was produced to calculate the estimated particle delivery rate for each ROI. For the FRAP analysis of PIN1-GFP lines, the images were process using FIJI software [43] as described by Walser et al. [60] and FRAP was calculated using the easyFRAP software [44].